Nanoscale

PAPER

View Article Online
View Journal | View Issue

Cite this: *Nanoscale*, 2020, **12**, 18171

Two-dimensional electronic devices modulated by the activation of donor-like states in boron nitride†

Sikandar Aftab, [a] Samiya,[b] Muhammad Waqas Iqbal,[c] Pragati A. Shinde,[a] Atteq ur Rehman,[d] Saqlain Yousuf,[e] Sewon Park[a] and Seong Chan Jun *[a]

A two-dimensional (2D) layered material-based p–n diode is an essential element in the modern semiconductor industry for facilitating the miniaturization and structural flexibility of devices with high efficiency for future optoelectronic and electronic applications. Planar devices constructed previously required a complicated device structure using a photoresist, as they needed to consider non-abrupt interfaces. Here, we demonstrated a WSe_2 based lateral homojunction diode obtained by applying a photoinduced effect in BN/WSe_2 heterostructures upon illumination *via* visible and deep UV light, which represents a stable and flexible charge doping technique. We have discovered that with this technique, a field-effect transistor (FET) based on p-type WSe_2 is inverted to n-WSe_2 so that a high electron mobility is maintained in the h-BN/n-WSe_2 heterostructures. To confirm this hypothesis, we deduced the work function values of p-WSe_2 and n-WSe_2 FETs by conducting Kelvin probe force microscopy (KPFM) measurements, which revealed the decline of the Fermi level from 5.07 (p-WSe_2) to 4.21 eV (n-WSe_2). The contact potential difference (CPD) between doped and undoped junctions was found to be 165 meV. We employed ohmic metal contacts for the planar homojunction diode by utilizing an ionic liquid gate to achieve a diode rectification ratio up to $\sim 10^5$ with n = 1. An exceptional photovoltaic performance is also observed. The presence of a built-in potential in our devices leads to an open-circuit voltage (V_{oc}) and short-circuit current (I_{sc}) without an external electric field. This effective doping technique is promising to advance the concept of preparing future functional devices.

Received 8th January 2020,
Accepted 25th January 2020

DOI: 10.1039/d0nr00231c

rsc.li/nanoscale

Introduction

Novel two-dimensional (2D) layered material-based nano-electronic devices are recognized as a potential alternative for silicon-based complementary devices. The primary achievement in obtaining an ultra-thin graphene (Gr) layer from bulk graphite *via* mechanical exfoliation encouraged the exploration of other 2D materials with promising applications in achieving various electronic and optoelectronic properties.[1,2] Particularly, tungsten diselenide (WSe_2)-based FETs have received remarkable devotion from experimentalists and have shown an exceptional on/off current ratio up to $\sim 10^7$ with a mobility of $\sim 100\ cm^2\ V^{-1}\ s^{-1}$.[3–5]

In addition, 2D material-based p–n junctions have also gained great attention from researchers due to their significant properties, for example charge transportation, band alignment, and optical absorption, for electronic and optoelectronic applications.[6,7] However, owing to the lack of controllable doping with respect to 2D materials, p–n diodes are constructed primarily by the stacking of van der Waals structures in homostructured or heterostructured phases.[8] Initially, electrostatic doping was induced to obtain diode-like behavior in graphene. However, graphene does not exhibit diode behavior owing to its zero band gap.[9] Electrostatic gate modulation is also employed in the case of transition metal dichalcogenide (TMDC)-based homojunction p–n diodes.[10–12] Nevertheless, they demonstrate a complicated structure and possess non-abrupt interfaces. Previously, chemical treatments required to

[a]*School of Mechanical Engineering, Yonsei University, Seoul 120-749, South Korea. E-mail: scj@yonsei.ac.kr*
[b]*Department of Environmental Engineering, Sejong University, 209 Neungdong-ro, Gwangjin-gu, Korea*
[c]*Department of Physics, Riphah International University, 14 Ali Road, Lahore, Pakistan*
[d]*Department of Electrical engineering, Sarhad University of Science and Information Technology, Peshawar, Pakistan*
[e]*Department of Physics, Sungkyunkwan University, Suwon, 440-746, South Korea*
†Electronic supplementary information (ESI) available. See DOI: 10.1039/d0nr00231c

control the carrier type in TMDCs were widely studied.[13,14] However, chemical or environmental effects significantly degrade the electrical properties of TMDC-based FETs and restrict the fundamental operation of these devices.[5,15–17] It is quite difficult to facilitate a stable n- or p-type conduction in nanoflakes as they frequently require substitutional, chemical doping or electrostatic gating.[18–20] Moreover, previously reported homojunction diodes employed similar metal electrodes for p and n-type materials and ignored the semiconductor and metal interface properties.[21,22] In several planar diodes, the contacts play a role that is not entirely related to their interfaces. The effects of low resistivity or ohmic metal contacts need to be explored to examine the intrinsic transport of TMDC-based devices.

Here, we demonstrated a planar WSe_2 homojunction p–n diode. The electron doping in p-type WSe_2 nanoflakes can be altered *via* an optical excitation of boron nitride (BN). The mechanism of electron photo-induced doping in WSe_2 is similar to the variation of the doping effect in Gr/BN heterostructures.[1,23] Such photo-induced doping in our planar device is triggered from point defects in multilayered crystalline BN flakes, and is entirely different from the photodoping effect witnessed in Gr flakes exfoliated on thick SiO_2 substrates.[22] The exfoliated BN flakes can also be used as a dielectric substrate for TMDC-based devices.[24,25] The KPFM measurements revealed the values of work function for p-type (5.6 eV) and n-type (4.21 eV) WSe_2 nanoflakes. The value of CPD between the two regions is estimated to be 165 meV. Although 2D material-based FETs with n-type conduction would make a Schottky contact with metals having higher values of work function, ohmic contacts are possible for metals with lower work function values to match with the conduction level of the n-type material. In contrast, 2D material-based FETs with p-type conduction exhibit opposite characteristics. Ohmic contacts are possible for metals with higher work function values to match with the valence level of the p-type material. In this study, we have discovered that p-WSe_2 and n-WSe_2 exhibit an ohmic contact with Pd/Au and Al/Au electrodes, respectively. In addition, we have examined the rectification ratio using different asymmetric electrodes of the pristine WSe_2 flake without the photodoping. The diode rectification ratio is much higher than the rectification ratio of the Pd/Au-(p-WSe_2)-Al/Au device. We have also confirmed that it is safe to reject the possibility that the photodoping effect is initiated from the intrinsic deep level trap state in WSe_2.

Materials and methods

Natural bulk crystals of WSe_2 and BN were mechanically exfoliated in a clean room using adhesive Scotch tape, and nanoflakes were transferred with the help of a transparent polydimethylsiloxane stamp using a dry-transfer technique. At first, the bottom gate electrodes of Cr/Au (4/40 nm) were constructed on SiO_2/Si substrates. Next, the BN flakes were transferred on the gate electrodes onto the SiO_2/Si substrates with the help of a micromanipulator, and lastly, the WSe_2 flakes were stacked vertically, making sure that they were partially lined up with the gate electrodes. The flakes were then placed on a hard plate to remove the H_2O vapor from exterior surfaces or the interfaces. For the fabrication of fine electrodes, the e-beam lithography method was used to create patterns. Furthermore, metal contacts, including Al/Au (6/80 nm) and Pd/Au (6/80 nm), were deposited on n-WSe_2 and p-WSe_2, respectively. The thickness of nanoflakes was measured using atomic force microscopy (AFM), while their structures were confirmed by Raman spectroscopy. The electrical and photovoltaic measurements were performed in a vacuum box at room temperature (300 K).

Results and discussion

The proposed device is schematically shown in Fig. 1a, wherein the BN/WSe_2 heterostructure is fabricated on top of the bottom gate electrode onto the SiO_2/p^+-Si substrate, and the optical image is shown in Fig. 1b. WSe_2 and BN flakes are produced by mechanical exfoliation using adhesive tape. Fig. S1(a and b) in the ESI† show the Raman spectra of BN, WSe_2, and BN/WSe_2 heterostructures. The Raman spectroscopy of the few-layered WSe_2 and multi-layered BN nanoflakes was performed with a laser (λ = 514 nm). Two peaks of WSe_2 can be seen in these spectra: A_{1g} mode at ~261.2 cm^{-1}, $E_{2g}{}^1$ mode at ~250.7 cm^{-1}, and E_{2g} mode at ~1363.9 cm^{-1} for BN. Fig. S1 (c and e)† show the typical AFM images of BN and WSe_2 flakes, while Fig. S1(d and f)† show the step profile height. The BN and WSe_2 nanoflakes exhibit a thickness of ~12.2 nm and ~3.6 nm, respectively.

2D materials, such as WSe_2, demonstrate semiconducting properties, and they may either show ambipolar behavior or p- or n-type conduction. The interface properties of 2D material-based FETs with metals are influenced by the conductive nature of the material. In this study, we discovered that Pd/WSe_2 or Al/WSe_2 interface properties could be either of the ohmic or the rectifying type depending on their work functions.

Initially, we fabricated BN/p-WSe_2 heterostructures using exfoliated nanoflakes on a bottom gate electrode, as shown in Fig. 1b. The ohmic contribution can be observed in the log scale of the I_D–V_D characteristic corresponding to the p-WSe_2 FET with Pd/Au electrodes (Fig. S2a†). Furthermore, to deduce the exact value of the work function of p-WSe_2, we performed the KPFM measurements. The work function value is calculated using the following equation:

$$\phi_{\text{P-WSe}_2} = \phi_{\text{tip}} + \text{CPD},$$

where $\phi_{\text{P-WSe}_2}$ denotes the work function of WSe_2 and ϕ_{tip} denotes the work function of the tip. In our case, the feedback system exists within the sample, because of which we used the positive sign in the above equation. The CPD for p-WSe_2 is estimated to be 0.275 eV from the KPFM data, and ϕ_{tip} = 4.8 eV.

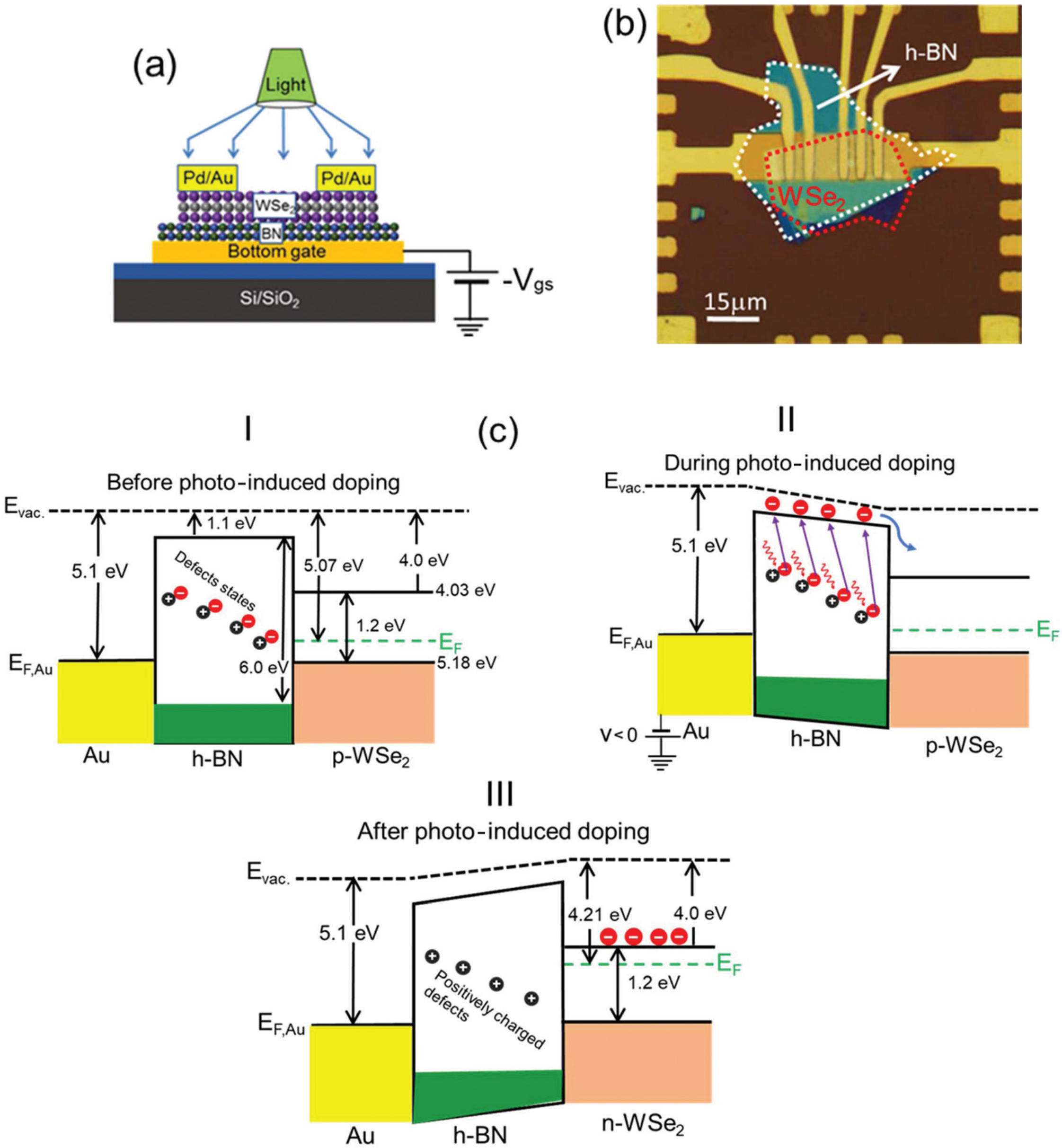

Fig. 1 (a) Schematic illustration of a BN/WSe_2 based FET under the illumination of light for obtaining a photo-induced effect. (b) Optical microscopy image of BN/WSe_2 with Pd/Au electrodes. (c) I: Schematic of the band structure of the BN/WSe_2 heterostructure before photo-induced doping; the work function value of p-WSe_2 is estimated to be 5.07 eV calculated using KPFM measurements. II: Schematic of the photo-induced process, in which the incident photons of light first excite the electrons from donor-like states in BN. The photoexcited electrons can be injected into WSe_2 under a negative gate stress voltage ($-V_{gs}$). III: The BN generates positively charged defects when V_{gs} and the light are off, and the work function value of n-WSe_2 is estimated to be 4.21 eV using KPFM measurements.

Therefore, the value of the work function for p-type WSe_2 is 5.07 eV, as shown in the band profile of Fig. 1c.

An exciting photodoping effect was established in WSe_2 based FETs to invert p-type conduction into n-type, where the BN/p-WSe_2 heterostructures were illuminated simultaneously with light of a wavelength of 220 nm for 7 min under a negative gate stress voltage (V_{gs}) of −10 V. From Fig. 2a, it is clear that the current on the electron side attains the same level, which demonstrates the electron doping effect. By increasing V_{gs} to −25 V, we observed that the current of the electron regime further increases, as shown in Fig. 2a. The photodoping treatment inverts WSe_2 with p-type to an n-type semiconductor. Moreover, the I_D–V_D characteristic with non-ohmic contribution obtained as a result of Schottky contacts at the interface of n-type WSe_2 with Pd/Au can be observed in the log scale of Fig. S2b.† Furthermore, the rectification ratio declines from 4.5 to 3.1, once the back-gate voltage (V_{bg}) is changed at the n-WSe_2/(Pd/Au) junction from −15 to +15 V (Fig. S2b†). The work function calculated using the KPFM measurements after photodoping is estimated to be ~4.21 eV, as shown in

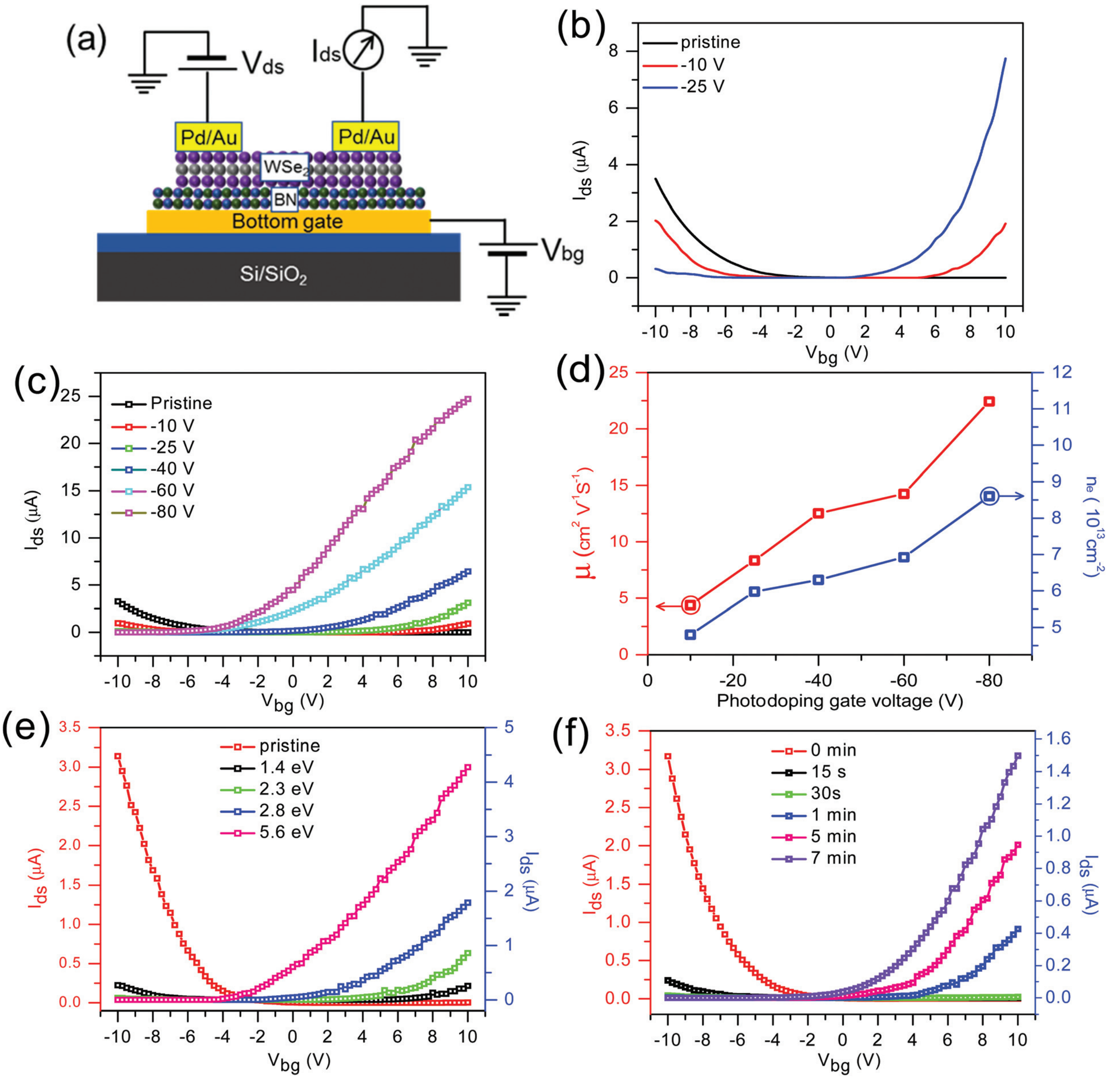

Fig. 2 (a) Schematic illustration of a BN/WSe_2 based FET after the photo-induced effect. (b) Transfer characteristics of pristine and doped BN/WSe_2 FET devices at V_{ds} = 0.5 V with a light of photon energy 5.6 eV for the illumination period t = 7 min at V_{gs} = −10 V and −25 V. The transfer curve indicates that p-WSe_2 has transformed from hole domination to electron domination (n-WSe_2). (c) Transfer characteristics of the BN/WSe_2 FET device with respect to V_{gs} for t = 5 min at V_{ds} = 0.5 V. The energy of incident photons is 2.3 eV. (d) Plot of electron concentration and mobility as a function of photo-induced gate voltage. (e) Transfer characteristics of the BN/WSe_2 based FET device at V_{ds} = 0.5 V with a different energy of incident photons for t = 5 min at V_{gs} = −10 V. (f) Transfer characteristics of the BN/WSe_2 based FET device at V_{ds} = 0.5 V for varied illumination times with an incident photon energy of 2.3 eV at V_{gs} = −10 V.

Fig. 1c. The photo-induced effect in WSe_2 has consequently modified the work function. It is observed that the value of the work function for WSe_2 declines (5.07 to 4.21 eV) as the p-type conduction is changed to n-type (Fig. 1c). The mechanism of photo-induced doping is initiated in the BN/p-WSe_2 heterostructures because of the photosensitive excitation of the defect states or the point defects in BN nanoflakes. The incident photons of light can excite defect states (or donor-like states)[26] in BN, as shown in Fig. 1c, which illustrates the photo-induced electron doping in BN/p-WSe_2 heterostructures. Upon illumination, the electrons of the point defects inside BN are stimulated to the conduction band. The excited electrons entered into WSe_2 under $-V_{gs}$. The localized ionized point defects in BN are positively charged, which can eliminate the influence of the electric field on BN throughout the process of photo-induced doping. The elimination of positively charged defects remains till the electric field in BN vanishes, and the ionized point defects remained in the interior of BN.[26]

The positive ionized point defect charges are observed inside BN, even if both the light and V_{gs} are switched off, which demonstrates a stable photo-induced doping effect in WSe_2.

Additionally, we validated the effect of the electron-photo-induced process on BN/WSe_2 heterostructures by varying parameters, such as V_{gs} (Fig. 2c), photon energy (Fig. 2e), and light exposure duration (Fig. 2f). It is clear from the results that our devices have demonstrated an enhanced electron-photo-induced effect for all the aforementioned parameters. The dominant effect can be observed with modulation in the photo-induced gate voltage, as shown in Fig. 2c. The dominant electron doping effect establishes that the doping level of electrons in WSe_2 nanoflakes could be modified by increasing V_{gs}. The carrier concentration of electrons (n_e) can be calculated by using the following relationship:

$$n_e = -\frac{C_g(V_g - V_{th})}{e},$$

where C_g is the gate capacitance of BN flakes, which can be calculated by $C_g = \frac{\varepsilon_o \varepsilon_r}{d}$, where ε_o is the permittivity constant and d is the thickness of BN flakes. The value of the dielectric constant for a multi-layered BN flake is ε_r = 4,[27] and C_g = ~2.90 × 10^{-7} F cm^{-2} for BN with a thickness of 12.2 nm. V_{th} is the threshold voltage for electron transport, V_g is the back-gate voltage, and e is the electronic charge. For example, the electron concentration was derived as ~8.6 × 10^{13} cm^{-2} at (V_{gs} = −80 V). The mobility (μ_{FE}) of n-WSe_2 in a two-terminal FET configuration can be calculated using the following equation:

$$\mu_{FE} = \frac{L}{W}\left(\frac{dI_{ds}}{dV_{bg}}\right)\frac{1}{C_g V_{ds}},$$

where W is the width and L is the length of the channel, the value of C_g for the BN substrate is ~2.90 × 10^{-7} F cm^{-2}, and $\frac{dI_{ds}}{dV_{bg}}$ is the slope of the linear part of the transfer plot. For instance, the electron mobility was estimated to be ~22 cm^2 V^{-1} s^{-1} for V_{gs} = −80. The carrier concentration (n_e) and electron mobility (μ_e) are shown in Fig. 2d.

Owing to the importance of photo-induced doping in WSe_2, planar devices were assembled using a random doping strategy with a free photoresist, unlike previously reported homojunction diodes that required a photoresist to modify the doping level.[28,29] Moreover, this method does not affect the properties of the metal electrodes in this device. The stability of n-type conduction in WSe_2 is observed over 50 days, as shown in Fig. S5.†

This lateral WSe_2 p–n diode was constructed on a thick BN flake having two bottom gate electrodes on the Si/SiO_2 substrate (Fig. 4b). While performing photodoping by using deep UV light having an energy of 5.6 eV for 5 min at V_{gs} = −40, half of the area of the WSe_2 flake was inverted to n-type, while half of the area remained p-type. The KPFM measurements were performed to determine the CPD value between the doped and undoped regions of WSe_2 using the highly doped Si tips under ambient conditions. A CPD value of approximately 165 meV is observed between p-WSe_2 and n-WSe_2 on the BN substrate (Fig. 3). The value of potential difference in our case is greater than that of the lateral WSe_2 homojunction diode (~55 mV) obtained based on helium ion irradiation.[30] It is comparable to that of the WSe_2 homojunction (~200 mV) obtained by H_2 plasma treatment for an n-type doping process.[31]

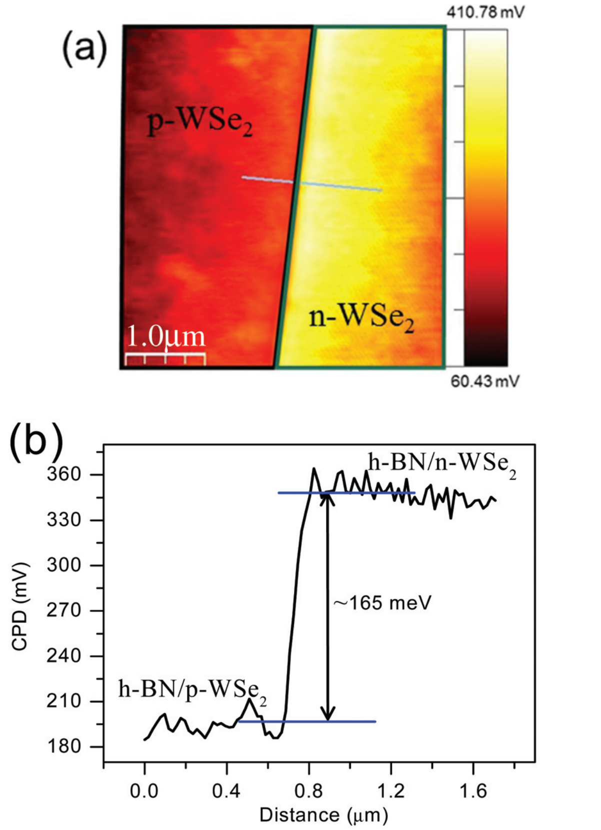

Fig. 3 (a) KPFM image of the WSe_2 flake at V_{gs} = −40 V. The line scans are denoted by the white line in the KPFM image. (b) The corresponding step profile height from the KPFM image as indicated. The value of contact potential difference between BN/p-WSe_2 and BN/n-WSe_2 is approximately 165 meV.

Fig. 4a shows the schematic diagram of a planar p–n diode, while Fig. 4b shows an optical image. The metals Al/Au and Pd/Au were deposited on the n-WSe_2 and p-WSe_2 layers, respectively. The I_D–V_D characteristics of n-WSe_2 and p-WSe_2 demonstrate a linear behavior, thereby confirming the low resistivity of the metal contacts, as shown in Fig. S4.† Individual n-WSe_2 and p-WSe_2 flakes were inspected for their transfer characteristics, and the results obtained are shown in Fig. 4c. We examined the gate-dependent rectifying performance of the planar homojunction diode by utilizing the ionic liquid gating effect, as FETs based on ionic liquid gates have been widely studied owing to their small operational voltage.[32–34] Fig. 4d shows the typical rectifying behavior of the planar WSe_2 homojunction diode under the influence of a low top gate voltage (V_{ILg}) changed from −2 to +2 V in a step of 0.5 V. The diode rectification behavior on a linear scale can be seen in Fig. S3.† It is observed from this figure that as V_{ILg}

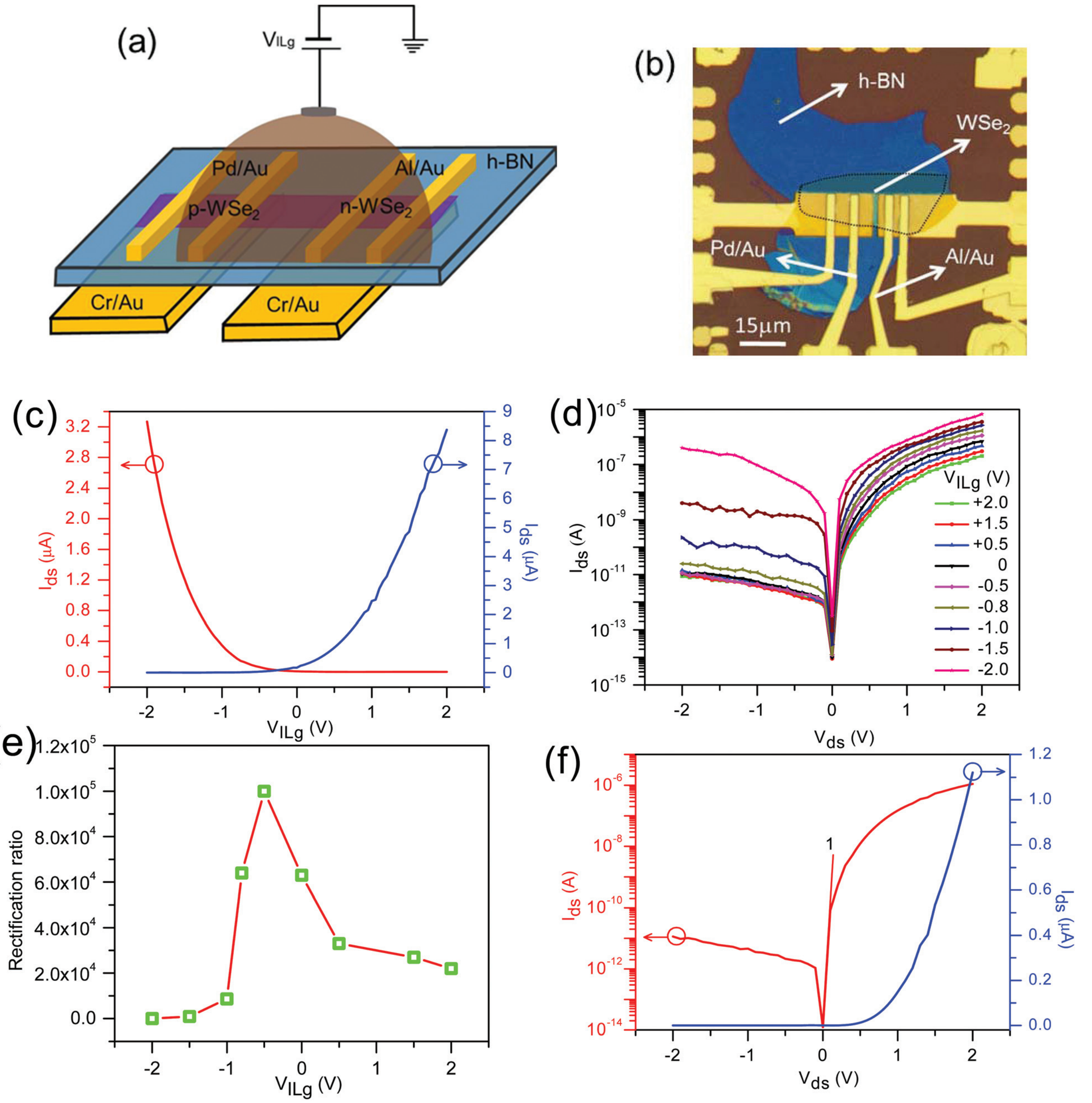

Fig. 4 (a) Schematic illustration of the lateral WSe_2 p–n diode. (b) Optical image of the p–n diode. The right WSe_2 channel on BN is electron-doped, while the one on the left remains pristine. (c) Transfer curves of p-WSe_2 and n-WSe_2 at V_{ds} = 0.5 V as a function of V_{bg}. (d) Gate-dependent rectifying effect of the diode in the log scale. (e) Rectification ratio of the diode as a function of top gate ionic liquid gate voltage. (f) Ideality factor of the device at V_{ILg} = −0.5 V.

increases from −2 to −0.5 V, the current values decline proportionally in the forward and reverse bias regions; however, these values decline much more rapidly in the negative bias region than on the positive side, which produces a dominant change in the rectification ratio of up to ~1.0×10^5, as shown in Fig. 4e. When V_{ILg} increases further from −0.5 to +2 V, it can be observed that the reverse current is almost unaffected, while the current in the forward regime continues to decrease, causing a decline in the rectification ratio (Fig. 4d). The ionic liquid gate-dependent rectification behavior of the lateral WSe_2 diode is due to the tunable built-in potential barrier at the homointerface of n-WSe_2 and p-WSe_2 under the influence of an external electric field. The transfer curve (I_{sd}–V_{ILg}) is divided into four regimes by tuning V_{ILg} (Fig. S7a†). In the transfer curve, the four regimes are demarcated by a hump with two valleys. This implies that the diode functions exist in the regimes p–p$^+$, p–n$^-$, p$^-$–n, and n–n$^+$. In the p–p$^+$ junction, the Fermi level of WSe_2 is moved downward, nearer to the valence band (Fig. S7b†), under the influence of a high negative gate bias, and the holes become dominant in both the channels, that is in the doped n-WSe_2 and undoped p-WSe_2. Furthermore, the device exhibits p-type semiconducting characteristics (Fig. S7a†). With an increase in the gate voltage, the Fermi level moves up nearer to the bandgap (Fig. S7b†), and the electrons become intensely dominant in the doped channel of WSe_2 owing to the creation of either one p–n$^-$ or p$^-$–n junction. This improves the built-in potential at the homointerface and causes an enhancement in the diode performance. When the value of greater positive gate bias increases further, the Fermi level enters into the conduction band (Fig. S7b†); the electrons become dominant in both the channels, *i.e.* in the doped n-WSe_2 and undoped p-WSe_2, and the device then functions in the n–n$^+$ junction and demonstrates an n-type semiconducting behavior (Fig. S7a†).

In addition, we have examined the rectification ratio using different asymmetric electrodes of the pristine WSe_2 flake without the photodoping. The diode rectification ratio is much higher (~6.3×10^4) at $V_{ILg} = 0$ V (Fig. 4e and f) than the rectification ratio (~59) of the Pd/Au-(p-WSe_2)-Al/Au device at $V_{bg} = 0$ without doping (Fig. S6†). When the p-WSe_2 channel itself was examined, no rectification behavior was observed with Pd/Au contacts, as shown in Fig. S4a.† Similarly, no rectification effect was observed in the n-WSe_2 channel with the Al/Au contacts, as shown in Fig. S4b.† In conclusion, the rectification in our diode is only due to the influence of the junction. Furthermore, to exclude the probability that the photodoping effect originated from the intrinsic deep level trap state in WSe_2, we performed an experiment. We fabricated devices by stacking WSe_2 nanoflakes on a thick BN flake with a part of its area placed on BN and the remaining area on SiO_2. The heterostructure of BN and WSe_2 was simultaneously illuminated under light and by applying $-V_{gs}$, and it was found that only a portion of the p-type WSe_2 flake that is placed on BN was inverted to n-WSe_2 during the photodoping treatment, while the area of the flake that is placed on SiO_2 remained p-type. This experiment confirmed that the photodoping effect does not originate from the intrinsic deep level trap state in WSe_2.

The ideality factor (n) of the diode was extracted by fitting to the equation[35,36] as follows:

$$I_D = I_S\left[\exp\left(\frac{qV}{nk_BT}\right) - 1\right],$$

where I_D is the diode current, I_S is the reverse saturation current, V is the applied voltage, q is the charge on electrons, T is the temperature, and k_B is Boltzmann's constant. For voltages > k_BT, the above equation becomes

$$\ln(I_D) = \ln(I_S) + \left(\frac{q}{nk_BT}\right)V.$$

The value of n is extracted to be ~1.0 at a gate bias of −0.5 V, as shown in Fig. 4f.

We further explored the optoelectronic response of the lateral WSe_2 diode using a laser light with $\lambda = 530$ nm. Fig. 5a shows the photovoltaic characteristics of this lateral WSe_2 diode. We calculated the photovoltaic parameters such as photoresponsivity $(R) = \frac{I_{ph}}{P_{laser\times A}}$ and external quantum efficiency $(\mathrm{EQE}) = R\frac{hc}{e\lambda}$, where $I_{ph} = I_{illumination} - I_{dark}$, laser power $P_{laser} = 10$ mW cm^{-2}, $\lambda = 530$ nm, and A is the junction area, c the speed of light, q the charge on electrons, and h is Planck's constant.[37,38] We deduced that R of the WSe_2 diode is 5.1 A W^{-1}, which is much greater than that of the $MoTe_2$-based homojunction diode.[39] Furthermore, it is observed from Fig. 5b that under different powers of light illumination, the I_D–V_D curves of the device do not pass through the zero points of voltage and current, even when there is no applied voltage. The presence of a built-in potential in our device leads to V_{oc} and I_{sc} without an external electric field (Fig. 5b). The detected phenomenon is the distinct feature of lateral diodes, as compared to photodetectors[40–42] or diodes based on mixed-dimensional heterostructures.

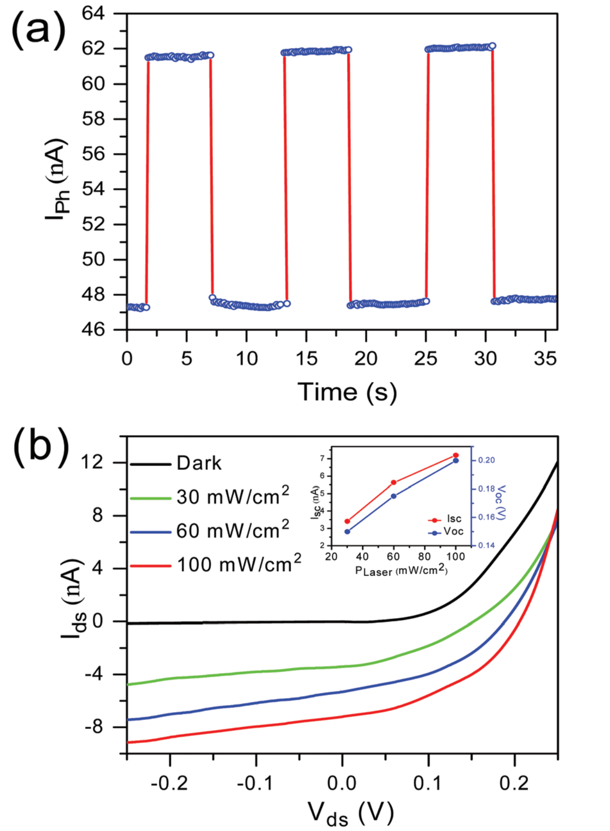

Fig. 5 Photoresponse of a WSe_2 homojunction p–n diode. (a) Photocurrent of the diode at $V_{ds} = 0.5$ V under green laser light illumination between the ON and OFF states. (b) Output I_D–V_D characteristics of the diode under dark and light illumination. The inset shows V_{oc} and I_{sc} as a function of the laser power.

Conclusion

In summary, we demonstrated a WSe_2 homojunction diode by applying the photo-induced effect in BN/WSe_2 heterostructures under the illumination of visible and deep UV light. It was revealed that with this photo-induced doping technique, FETs based on p-type WSe_2 were inverted to n-WSe_2, which can maintain a high electron mobility in h-BN/n-WSe_2 heterostructures. To confirm this hypothesis, KPFM measurements were performed to deduce the work function values of p-WSe_2 and n-WSe_2 FETs as 5.07 eV and 4.21 eV, respectively. The KPFM measurements revealed the modification of the Fermi level in WSe_2 owing to electron doping from donor-like states of h-BN under illumination because of the photo-induced gate voltage. They were also used to deduce the value of CPD between the doped and undoped junctions, which was estimated to be 165 meV. We used ohmic metal contacts for the planar homojunction diode by utilizing the ionic liquid gate and achieved a diode rectification ratio ($\sim 10^5$) with $n = 1$. In addition, excellent photovoltaic performances were demonstrated by these devices. Therefore, we consider that a stable and flexible charge doping technique within a single flake can be effective for electronic applications.

Conflicts of interest

The authors declare no competing financial interests.

Acknowledgements

This work was supported by the national research foundation of Korea (NRF) grant funded by the Korea government (MIST) (No. NRF 2019R1A2C2090443 and NRF-2017M3A7B4041987). This work is also funded by the Higher Education Commission (HEC) of Pakistan under the National Research Program for Universities (NRPU) with project no. HEC/R&D/NRPU/2017/7876.

References

1 S. Aftab and J. Eom, *2D Mater.*, 2019, **6**, 035005.
2 K. S. Novoselov, A. K. Geim, S. V. Morozov, D. Jiang, Y. Zhang, S. V. Dubonos, I. V. Grigorieva and A. A. Firsov, *Science*, 2004, **306**, 666–669.
3 W.-M. Kang, S. Lee, I.-T. Cho, T. H. Park, H. Shin, C. S. Hwang, C. Lee, B.-G. Park and J.-H. Lee, *Solid-State Electron.*, 2018, **140**, 2–7.
4 J. Kang, W. Liu, D. Sarkar, D. Jena and K. Banerjee, *Phys. Rev. X*, 2014, **4**, 031005.
5 H. Fang, S. Chuang, T. C. Chang, K. Takei, T. Takahashi and A. Javey, *Nano Lett.*, 2012, **12**, 3788–3792.
6 Y. Deng, Z. Luo, N. J. Conrad, H. Liu, Y. Gong, S. Najmaei, P. M. Ajayan, J. Lou, X. Xu and P. D. Ye, *ACS Nano*, 2014, **8**, 8292–8299.
7 W. Hu and J. Yang, *J. Mater. Chem. C*, 2017, **5**, 12289–12297.
8 S. Aftab, M. F. Khan, P. Gautam, H. Noh and J. Eom, *Nanoscale*, 2019, **11**, 9518–9525.
9 N. Stander, B. Huard and D. Goldhaber-Gordon, *Phys. Rev. Lett.*, 2009, **102**, 026807.
10 J. S. Ross, P. Klement, A. M. Jones, N. J. Ghimire, J. Yan, D. Mandrus, T. Taniguchi, K. Watanabe, K. Kitamura and W. Yao, *Nat. Nanotechnol.*, 2014, **9**, 268.
11 A. Pospischil, M. M. Furchi and T. Mueller, *Nat. Nanotechnol.*, 2014, **9**, 257.
12 B. W. Baugher, H. O. Churchill, Y. Yang and P. Jarillo-Herrero, *Nat. Nanotechnol.*, 2014, **9**, 262.
13 C. Han, Z. Hu, L. C. Gomes, Y. Bao, A. Carvalho, S. J. Tan, B. Lei, D. Xiang, J. Wu and D. Qi, *Nano Lett.*, 2017, **17**, 4122–4129.
14 M. S. Choi, D. Qu, D. Lee, X. Liu, K. Watanabe, T. Taniguchi and W. J. Yoo, *ACS Nano*, 2014, **8**, 9332–9340.
15 S. Roy, A. G. Joshi, S. Chatterjee and A. K. Ghosh, *Nanoscale*, 2018, **10**, 10664–10682.
16 A. C. Ferrari, F. Bonaccorso, V. Fal'Ko, K. S. Novoselov, S. Roche, P. Bøggild, S. Borini, F. H. Koppens, V. Palermo and N. Pugno, *Nanoscale*, 2015, **7**, 4598–4810.
17 H. Schmidt, F. Giustiniano and G. Eda, *Chem. Soc. Rev.*, 2015, **44**, 7715–7736.
18 N. Ubrig, S. Jo, H. Berger, A. F. Morpurgo and A. B. Kuzmenko, *Appl. Phys. Lett.*, 2014, **104**, 171112.
19 Y. Zhang, J. Ye, Y. Yomogida, T. Takenobu and Y. Iwasa, *Nano Lett.*, 2013, **13**, 3023–3028.
20 C. J. Benjamin, S. Zhang and Z. Chen, *Nanoscale*, 2018, **10**, 5148–5153.
21 J. Suh, T.-E. Park, D.-Y. Lin, D. Fu, J. Park, H. J. Jung, Y. Chen, C. Ko, C. Jang and Y. Sun, *Nano Lett.*, 2014, **14**, 6976–6982.
22 A. Nipane, D. Karmakar, N. Kaushik, S. Karande and S. Lodha, *ACS Nano*, 2016, **10**, 2128–2137.
23 P. Zomer, S. Dash, N. Tombros and B. Van Wees, *Appl. Phys. Lett.*, 2011, **99**, 232104.
24 L. Britnell, R. V. Gorbachev, R. Jalil, B. D. Belle, F. Schedin, M. I. Katsnelson, L. Eaves, S. V. Morozov, A. S. Mayorov and N. M. Peres, *Nano Lett.*, 2012, **12**, 1707–1710.
25 L. Britnell, R. Gorbachev, R. Jalil, B. Belle, F. Schedin, A. Mishchenko, T. Georgiou, M. Katsnelson, L. Eaves and S. Morozov, *Science*, 2012, **335**, 947–950.
26 L. Ju, J. Velasco Jr., E. Huang, S. Kahn, C. Nosiglia, H.-Z. Tsai, W. Yang, T. Taniguchi, K. Watanabe and Y. Zhang, *Nat. Nanotechnol.*, 2014, **9**, 348.
27 J. Wang, F. Ma and M. Sun, *RSC Adv.*, 2017, **7**, 16801–16822.
28 J. Y. Lim, A. Pezeshki, S. Oh, J. S. Kim, Y. T. Lee, S. Yu, D. K. Hwang, G. H. Lee, H. J. Choi and S. Im, *Adv. Mater.*, 2017, **29**, 1701798.
29 W. Luo, M. Zhu, G. Peng, X. Zheng, F. Miao, S. Bai, X. A. Zhang and S. Qin, *Adv. Funct. Mater.*, 2018, **28**, 1704539.
30 M. G. Stanford, P. R. Pudasaini, A. Belianinov, N. Cross, J. H. Noh, M. R. Koehler, D. G. Mandrus, G. Duscher, A. J. Rondinone and I. N. Ivanov, *Sci. Rep.*, 2016, **6**, 27276.
31 M. Tosun, L. Chan, M. Amani, T. Roy, G. H. Ahn, P. Taheri, C. Carraro, J. W. Ager, R. Maboudian and A. Javey, *ACS Nano*, 2016, **10**, 6853–6860.

32 P. R. Pudasaini, J. H. Noh, A. Wong, A. V. Haglund, S. Dai, T. Z. Ward, D. Mandrus and P. D. Rack, *ECS J. Solid State Sci. Technol.*, 2015, **4**, Q105–Q109.
33 S. Zhang, N. Sun, X. He, X. Lu and X. Zhang, *J. Phys. Chem. Ref. Data*, 2006, **35**, 1475–1517.
34 R. Misra, M. McCarthy and A. F. Hebard, *Appl. Phys. Lett.*, 2007, **90**, 052905.
35 D. A. Neamen, *Semiconductor physics and devices*, McGraw-Hill, New York, 1997.
36 T. Banwell and A. Jayakumar, *Electron. Lett.*, 2000, **36**, 291–292.
37 M. M. Furchi, A. Pospischil, F. Libisch, J. Burgdörfer and T. Mueller, *Nano Lett.*, 2014, **14**, 4785–4791.
38 L. Ye, H. Li, Z. Chen and J. Xu, *ACS Photonics*, 2016, **3**, 692–699.
39 S. Aftab, M. F. Khan, P. Gautam, H. Noh and J. Eom, *Nanoscale*, 2019, 9518–9525.
40 Z. Zheng, T. Zhang, J. Yao, Y. Zhang, J. Xu and G. Yang, *Nanotechnology*, 2016, **27**, 225501.
41 W. Zhang, M.-H. Chiu, C.-H. Chen, W. Chen, L.-J. Li and A. T. S. Wee, *ACS Nano*, 2014, **8**, 8653–8661.
42 R. K. Chowdhury, R. Maiti, A. Ghorai, A. Midya and S. K. Ray, *Nanoscale*, 2016, **8**, 13429–13436.